https://doi.org/10.5194/egusphere-2023-749
Preprint. Discussion started: 3 May 2023


# An Updated Modeling Framework to Simulate Los Angeles Air Quality. Part 1: Model Development, Evaluation, and Source Apportionment.

Elyse A. Pennington[1], Yuan Wang[2,3], Benjamin C. Schulze[4], Karl M. Seltzer[5], Jiani Yang[4], Bin Zhao[6,7], Zhe Jiang[8], Hongru Shi[9], Melissa Venecek[10], Daniel Chau[10], Benjamin N. Murphy[11], Christopher M. Kenseth[12], Ryan X. Ward[4], Havala O. T. Pye[11], and John H. Seinfeld[1,4]

[1]Department of Chemical Engineering, California Institute of Technology, Pasadena, CA 91125

[2]Department of Earth, Atmosphere, and Planetary Sciences, Purdue University, West Lafayette, IN 47907

[3]Division of Geological and Planetary Sciences, California Institute of Technology, Pasadena, CA 91125

[4]Department of Environmental Science and Engineering, California Institute of Technology, Pasadena, CA 91125

[5]Office of Air and Radiation, US Environmental Protection Agency, Research Triangle Park, NC 27711

[6]State Key Joint Laboratory of Environmental Simulation and Pollution Control, School of Environment, Tsinghua University, Beijing 100084, China

[7]State Environmental Protection Key Laboratory of Sources and Control of Air Pollution Complex, Beijing 100084, China

[8]Carbon Neutrality Research Center, Institute of Atmospheric Physics, Chinese Academy of Sciences, Beijing, China

[9]Key Laboratory of Middle Atmosphere and Global Environment Observation, Institute of Atmospheric Physics, Chinese Academy of Sciences, Beijing, China

[10]Modeling and Meteorology Branch, California Air Resources Board, Sacramento, CA 95814

[11]Office of Research and Development, US Environmental Protection Agency, Research Triangle Park, NC 27711

[12]Department of Chemistry, California Institute of Technology, Pasadena, CA 91125

Corresponding Authors: Yuan Wang (yuanwang@purdue.edu) and John H. Seinfeld (seinfeld@caltech.edu)

## Abstract

This study describes a modeling framework, model evaluation, and source apportionment to understand the causes of Los Angeles (LA) air pollution. A few major updates are applied to the Community Multiscale Air Quality (CMAQ) Model with high spatial resolution (1 km x 1 km). The updates include dynamic traffic emissions based on real-time on-road information and recent

https://doi.org/10.5194/egusphere-2023-749
Preprint. Discussion started: 3 May 2023


emission factors and secondary organic aerosol (SOA) schemes to represent volatile chemical products (VCP). Meteorology is well-predicted compared to ground-based observations, and the emission rates from multiple sources (i.e., on-road, volatile chemical product, area, point, biogenic, and sea spray) are quantified. Evaluation of the CMAQ model shows that ozone is well-predicted despite inaccuracies in nitrogen oxide ($NO_x$) predictions. Particle matter (PM) is underpredicted compared to concurrent measurements made with an aerosol mass spectrometer (AMS) in Pasadena. Inorganic aerosol is well-predicted while SOA is underpredicted. Modeled SOA consists of mostly organic nitrates and products from oxidation of alkane-like intermediate volatility organic compounds (IVOCs) and has missing components that behave like less-oxidized oxygenated organic aerosol (LO-OOA). Source apportionment demonstrates that the urban areas of the LA Basin and vicinity are $NO_x$-saturated (VOC-sensitive) with the largest sensitivity of $O_3$ to changes in VOCs in the urban core. Differing oxidative capacities in different regions impact the nonlinear chemistry leading to PM and SOA formation, which is quantified in this study.

## 1. Introduction

Air quality is influenced by particle- and gas-phase species which can impact human and environmental health. Particulate matter (PM), or aerosols, affect human health (Lim et al., 2012), climate (Intergovernmental Panel on Climate Change, 2014), and visibility (Hyslop, 2009). A major fraction of PM in urban areas is organic (Q. Zhang et al., 2007), which itself is largely secondary in nature (Jimenez et al., 2009). Secondary organic aerosol (SOA) comprises thousands of species which are formed via complex chemistry that also produces ozone ($O_3$). $O_3$ is an oxidant which can damage human (Nuvolone et al., 2018) and plant (Sandermann Jr, 1996) health. Reactive organic gases (ROG) are necessary precursors to these pollutants and span a range of properties, including vapor pressure and oxygen-to-carbon ratio. Volatile organic compounds (VOCs) and nitrogen oxides ($NO_x$) control $O_3$ and SOA formation, and semivolatile organic compounds (SVOCs) and intermediate volatility organic compounds (IVOCs) have high potential to form SOA (Robinson et al., 2007).

The Los Angeles Basin has a long history of air pollution resulting from substantial anthropogenic emissions and unique meteorology. On-road mobile emissions have historically been the most important source of atmospheric pollution in the LA Basin, but emissions have decreased as emissions control technologies (i.e., catalytic converters) have improved, vehicle fuel efficiencies have increased, and electric vehicles have become more prevalent (Khare & Gentner, 2018). Other sources of emissions have become more important, particularly VOC and SVOC emissions from volatile chemical products (VCPs). VCPs are consumer and industrial products that utilize evaporative organics (Seltzer et al., 2021) and can form SOA (Qin et al., 2021). Asphalt emissions can also form SOA, and are likely important in LA where the urban land fraction and temperatures are both high (Khare et al., 2020). In addition to organic emission reductions, $NO_x$ emissions from on-road vehicles have decreased. Moreover, $NO_x$ emissions from off-road vehicles have become almost equally important to on-road $NO_x$ emissions in LA (Khare & Gentner, 2018). As total emissions have decreased, ambient levels of most criteria pollutants have decreased, including $NO_x$, carbon monoxide (CO), and sulfur oxides ($SO_x$) (US EPA, 2013). However, $O_3$ in LA has increased in the past decade (US EPA, 2013) because of the nonlinear atmospheric chemistry leading to its formation (Seinfeld & Pandis, 2016); (Le et al., 2020). The LA Basin also displays a temperature inversion layer which leads to strong atmospheric stability with a low flow

https://doi.org/10.5194/egusphere-2023-749
Preprint. Discussion started: 3 May 2023


rate out of the Basin. The complex interactions between emissions, meteorology, and chemistry will be investigated in this study.

Predicting air quality using chemical transport models (CTMs) is challenging. Developing a model that best represents the complexity of atmospheric chemistry—particularly SOA formation—in a reasonable computation time involves a tradeoff in chemical details. Models exist which represent gas-phase and heterogeneous chemistry (e.g., Carter, 2010; Yarwood et al., 2010; Goliff et al., 2013, Keller & Evans, 2019), and researchers have traditionally modeled SOA formation from VOC oxidation (e.g., Odum et al., 1996; Carlton et al., 2010). An active area of research is the oxidation of SVOCs and IVOCs, which likely yield higher SOA than VOCs due to their lower volatility (e.g., Donahue et al., 2011; Murphy et al., 2017; Gentner et al., 2017). It is well-documented that SOA tends to be underpredicted in Community Multiscale Air Quality (CMAQ) model (Appel et al., 2021) unless an empirical representation of anthropogenic SOA is introduced (Murphy et al., 2017), so a goal of model improvement is to increase SOA mass with improved understanding of sources and physiochemical processes. Representing the correct sources of SOA in a process-based approach is critical for model applications designed to inform control strategies. Recent works have developed new models to represent SOA formation from VCPs (Pennington et al., 2021) and mobile sector IVOCs (Lu et al., 2020), which reduced model SOA bias. The predicted chemistry leading to pollutant formation is highly nonlinear (Seinfeld & Pandis, 2016), and is additionally influenced by emission inventories that typically have high uncertainties (Qin et al., 2021); (Khare & Gentner, 2018). Recent work has improved the estimation of emission rates of VCP VOCs (Seltzer et al., 2021), on-road VOCs, $NO_x$, PM, and CO (California Air Resources Board, 2018), and on-road IVOCs (Zhao et al., 2016).

Detailed observational data that can be used to constrain model parameters governing chemical transformations is often lacking. While pollutants like $O_3$, $PM_{2.5}$, and $NO_2$ are regularly monitored throughout the United States (US EPA, 2013), these sites tend to be sparsely distributed. Components of $PM_{2.5}$ are generally only available on a daily-integrated basis, preventing diagnostic separation of daytime vs nighttime chemistry. Measurements of radical species and specific VOCs are only obtained during field campaigns, which are limited to a small region during a short time duration because they are very expensive to carry out. Even though the lack of in situ data makes it difficult to parameterize or evaluate models, it also underscores the importance of models. Models fill in the spatiotemporal gaps in our measurements and allow us to predict important air quality impacts.

The modeling period in this study covers April 2020, during the strict COVID-19 lockdown regulations in LA. On-road vehicle miles traveled (VMT) declined significantly during this month as many people remained at home (Caltrans, 2020), and this altered the composition of anthropogenic emissions and resulting pollutant levels (Parker et al., 2020). However, this period also experienced several weather patterns that are unusual to springtime months in LA, namely a rainy period and a very hot period. Untangling the relative impacts of decreased emissions versus meteorology is feasible using CTMs.

In the first part of this work, we use the CMAQ model to understand the current air quality of the Los Angeles Basin. Model inputs to CMAQ are developed to represent meteorology and emissions in 2020 and are evaluated against available data. CMAQ model predictions are presented throughout the Basin, while source apportionment studies describe the important sources of emissions. SOA formation in Pasadena is compared to detailed ground-based measurements. In Part 2 of this work, documented in a second article, the sensitivity of pollutants to reduced on-road

https://doi.org/10.5194/egusphere-2023-749
Preprint. Discussion started: 3 May 2023


and VCP emissions are further explored. The relative importance of emissions and meteorology in dictating $O_3$ and PM concentrations during the COVID-19 pandemic are also investigated. The simulations investigated in part 2 can represent future emission scenarios and provide insight on helpful policies to mitigate air quality.

## 2. Methods

### 2.1 Model Development

The model framework is summarized in Figure 1 and detailed descriptions of each component are described below. CTM inputs include meteorology, emissions, chemical boundary conditions, and grid information. The CTM uses these inputs to predict concentrations which will be compared to hourly or daily observed data throughout the domain and specifically in Pasadena.

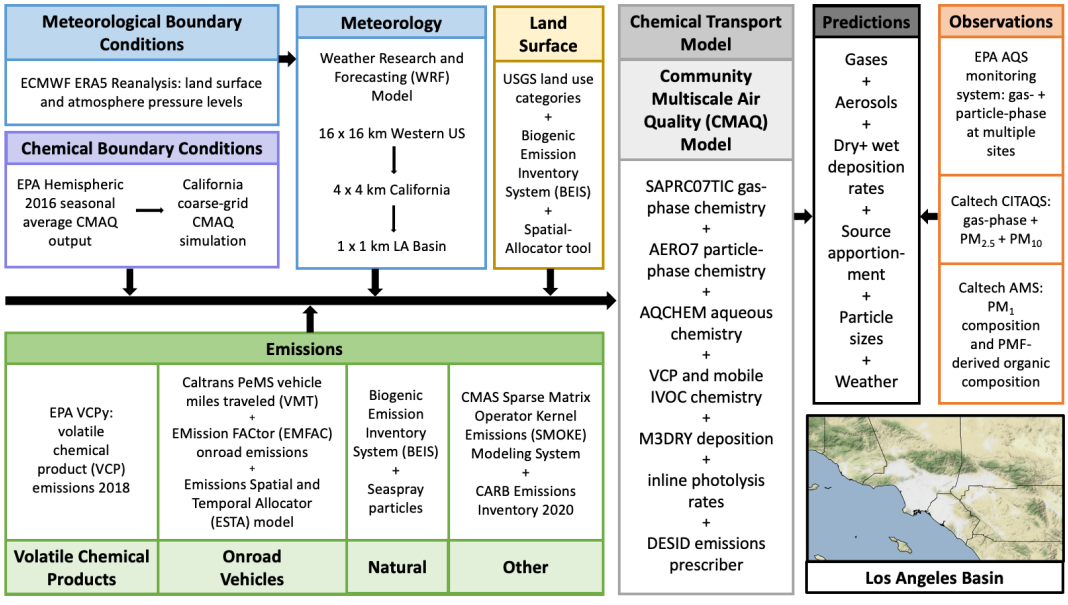


Figure 1: Model framework describing the inputs to CMAQ, CMAQ configuration, observational data, and modeling domain.

#### 2.1.1 Chemical Transport Model

We use CMAQ version 5.3.2 (US EPA, 2020), which is documented and evaluated in Appel et al. (2021). The gas-phase chemical mechanism used here is SAPRC07TIC (Carter, 2010) (Xie et al., 2013), the organic aerosol-phase chemical mechanism is AERO7 (Pye et al., 2013; Pye et al., 2017; Murphy et al., 2017; Xu et al., 2018; Qin et al., 2021), the inorganic aerosol-phase chemical mechanism is ISORROPIA II (Fountoukis & Nenes, 2007), and the aqueous-phase chemical mechanism used is the Asymmetric Convection Model (ACM) version 2 (Binkowski & Roselle, 2003); (Pleim, 2007). The M3Dry module is the air-surface exchange module used to represent the dry deposition of gas- and particle-phase species (Pleim & Ran, 2011; Appel et al., 2021) and uses the Noah land surface model (Alapaty et al., 2008). The Detailed Emissions Scaling, Isolation, and Diagnostic (DESID) module within CMAQ (Murphy et al., 2021) was used to modify emissions and in our source apportionment sensitivity simulations. The

https://doi.org/10.5194/egusphere-2023-749
Preprint. Discussion started: 3 May 2023


SAPRC07TIC_AE7 chemical mechanism used here was updated to include the emissions and chemistry of VCP species (Pennington et al. (2021) and IVOCs from on-road mobile sources (Lu et al. 2020). The organic aerosol (OA) chemical mechanism is summarized in Figure S1.

### 2.1.2 Meteorology

Meteorological simulations are performed using the Weather Research and Forecasting (WRF) Model (Skamarock et al., 2008) version 4.2. Climatological input data are provided from the ERA5 Reanalysis Dataset (Hersbach et al., 2018, p. 5), which contains hourly data on a 0.25° x 0.25° grid at the surface and on 37 pressure levels from 100 to 1 hPa. The WRF configuration uses three nested domains to resample and simulate the meteorological variables from the input resolution to 16-km, 4-km, and then 1-km resolution (Figure 2A). The innermost 1 km x 1 km domain is the region of interest in this study and referred to as the LA domain (Figure 2A, C).

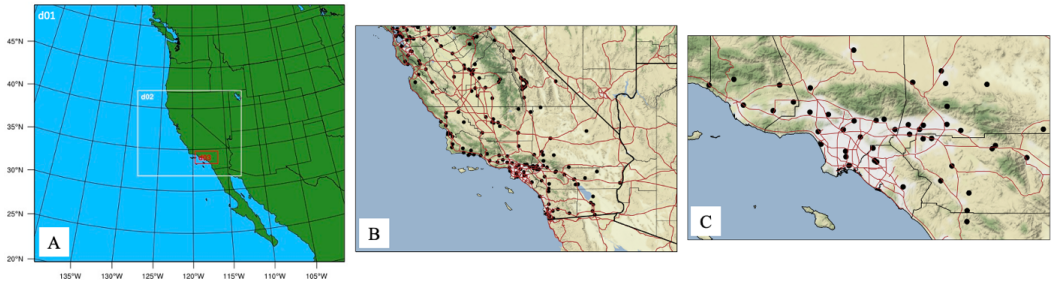


Figure 2: A) Three nested domains used in the WRF simulations. d01 has a horizontal resolution of 16 km, d02 has a resolution of 4 km, and d01 has a resolution of 1 km. B) California 4 x 4 km coarse-resolution domain. C) LA 1 x 1 km fine-resolution domain. Thick black lines are state borders and thin black lines are county borders. Black dots represent EPA AQS sites and red lines are freeways.

### 2.1.3 Emissions

On-road vehicles can be separated into two categories, light duty and heavy duty, based on the weight of the vehicle. Light duty vehicles are smaller, tend to be passenger cars, and tend to use gasoline fuel. On the other hand, heavy duty vehicles are larger, tend to be used for commodity transport, and tend to use diesel fuel. These categories are represented separately in the model because there has been historical interest in understanding the class of vehicles and fuel to target for emissions regulations (e.g., Bahreini et al., 2012; Ensberg et al., 2014; Gentner et al., 2017; Lu et al., 2020). Additionally, because of the different uses of these types of vehicles, their driving and therefore emissions patterns differ spatially and temporally.

On-road mobile emissions are represented by the EMission FACtor (EMFAC2017) emissions inventory and model projected to year 2020 (California Air Resources Board, 2018). The projection to year 2020 includes 2020-specific meteorological effects on emission rates. The Emissions Spatial and Temporal Allocator (ESTA) model uses 1 km x 1 km spatial surrogates and California Vehicle Activity Database (CalVAD) temporal surrogates (Ritchie & Tok, 2016) to calculate hourly, gridded emissions on the LA domain. The speciation profiles used in ESTA include the surrogate NMOG (non-methane organic gases), which provides diagnostic information but is not used by the chemistry in CMAQ. To estimate emissions of alkane-like IVOC emissions, the unspeciated fraction of NMOG was used with information from Lu et al. (2020).

https://doi.org/10.5194/egusphere-2023-749
Preprint. Discussion started: 3 May 2023


EMFAC and ESTA do not capture the effect of COVID-19 on vehicle use, so we modified the on-road emissions to include those changes. The California Performance Measurement System (PeMS) uses in-situ detectors distributed throughout California to measure vehicle usage metrics (Caltrans, 2020). One such metric is vehicle miles traveled (VMT), which measures the miles traveled by different vehicle types, e.g., light and heavy duty vehicles. VMT changed directly in response to COVID-19 policies and human behavior changes, so it can be used to reduce on-road emissions in response to the pandemic (Yang et al., 2021). VMT data were summed for all PeMS monitoring sites in the LA domain, separated into heavy duty and light duty vehicles (Figure 3a-b). VMT January through March (pre-pandemic) was relatively constant. These values were averaged and used as the baseline VMT, represented by the dashed black lines. VMT decreased in March as COVID-19 stay-at-home policies were implemented. VMT reached its lowest value in April and then slowly increased towards the baseline value. All weekly-averaged VMT values were divided by the baseline VMT value to obtain scaling factors which are a proxy for declining vehicle emissions resulting from the pandemic (Figure *3*c). The VMT scaling factors are not identical for light duty and heavy duty vehicles, consistent with the rationale for separating these vehicle types. Light duty VMT decreased the most, since the pandemic primarily decreased the use of personal vehicles, with a lesser decrease of industrial transport vehicles' (i.e. heavy-duty vehicles) use.

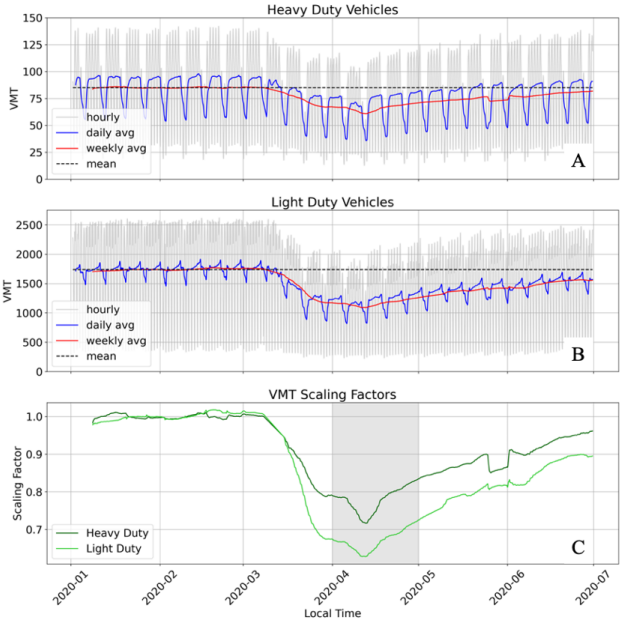


Figure 3: Hourly (gray), daily-averaged (blue), and weekly-averaged (red) VMT data (Caltrans, 2020) for A) heavy duty vehicles and B) light duty vehicles. VMT averaged January 1– March 1, 2020 is represented by the dashed black line. C) Weekly-averaged VMT divided by the January–March mean for heavy duty (dark green) and light duty (light green) vehicles. The gray shaded area covers the modeling period: April 1–30, 2020.

VCP emissions are predicted using the VCPy model framework (Seltzer et al., 2021). VCPy version 1.1 (Seltzer et al., 2022) was used to calculate VOC emission rates for 2018 over

https://doi.org/10.5194/egusphere-2023-749
Preprint. Discussion started: 3 May 2023


the contiguous United States (CONUS) on a 4 km x 4 km grid, which were re-gridded to 1 km x 1 km to fit the LA domain grid. The year 2018 emissions are assumed to be representative of year 2020 emissions within the range of uncertainty present in VCPy.

Natural emissions are treated in-line in CMAQ using land surface descriptive files generated using the Spatial-Allocator tool (US EPA, 2017/2022). Gas-phase biogenic emissions and particle-phase sea spray emissions are modeled using the Biogenic Emission Inventory System (BEIS) version 3.6.1 (Bash et al., 2016). Lightning $NO_x$ and windblown dust emissions are not turned on in the model.

All other emissions are calculated using the California Air Resources Board (CARB) emissions inventory (CARB, 2020). The emissions inventory includes data from sources including off-road vehicles and equipment, agriculture, oil and gas production, industrial, and other sources. Annual emission rates were calculated for base year 2017 and scaled to year 2020 using the California Emissions Projection Analysis Model (CEPAM) growth and control data (CARB, 2020). The inventory is processed in the Sparse Matrix Operator Kernel Emissions (SMOKE) model version 4.8 (CMAS, 2020) using spatial and temporal surrogates from 2019. SMOKE calculates both gridded area source emissions as well as individual point source emissions, and their sum will be referred to as area+point emissions.

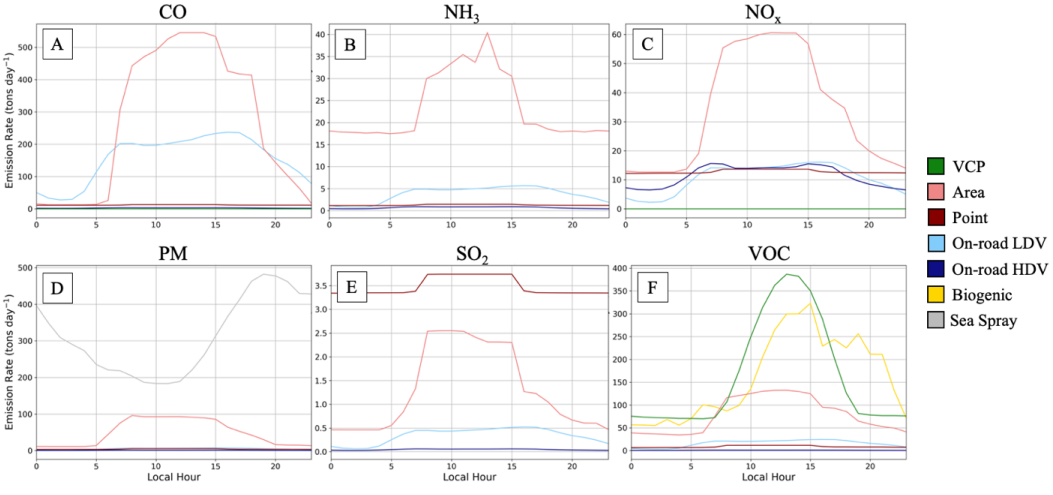


Figure 4: Diurnal variations of emission rates averaged April 1–30, 2020 and summed over the LA domain (with all ocean-covered cells removed) from all emission sources for A) CO, B) $NH_3$, C) $NO_x$, D) PM, E) $SO_2$, F) VOC.

Emission rates and the importance of each emission source vary by pollutant and region. Domain-wide emission rates are given in Figure 4 and the spatial distribution of emissions is given in Figures S2-7. All anthropogenic emissions peak during midday when people are most active. Biogenic VOC and NO emissions also peak midday corresponding to temperature. In contrast, sea spray emissions peak overnight as temperatures decrease and winds increase. Sea spray emissions are only located in the surf zone along the coastline (Figure S5). Biogenic sources emit significant VOCs, comparable to those from VCPs. However, VCP emissions are largest over urban areas while biogenic VOC emissions are largest over remote regions (Figure S7), and so will impact pollutant formation regionally. Area and point sources emit large amounts of all pollutants and

https://doi.org/10.5194/egusphere-2023-749
Preprint. Discussion started: 3 May 2023


comprise a variety of sources (Figures S8-9). On-road vehicles emit large amounts of CO (Figure 4), but total CO emissions are dominated by off-road vehicles (Figure S8). On-road vehicles also emit significant $NO_x$ (Figure 4), similar in quantity to the individual area+point sources (i.e., boats, off-road, and trains) given in Figure S8.

### 2.1.4 Initial & Boundary Conditions

A nested modeling setup was used to provide the boundary conditions for the Los Angeles Basin. The Los Angeles Basin is represented by the domain shown in Figure 2C, has a resolution of 1 km x 1 km, and is the domain of interest for this project. The initial and boundary conditions for the LA domain were provided by a coarse-resolution CMAQ simulation performed over a larger domain (Figure 2B). The outer domain covering southern and central California has a resolution of 4 km x 4 km and its air quality was simulated using the WRF and CMAQ scenarios described in Sections 2.1.1-2.1.2. The emissions for this domain match the emissions described in (Jiang et al., 2021). Publicly-available seasonal average hemispheric CMAQ output was used as initial and boundary conditions for the California domain (Hogrefe et al., 2021). The CMAQ predictions from the coarse-resolution California domain were used as initial and boundary conditions for the inner, finer-resolution LA domain.

## 2.2 Observational Data

Observational data throughout the modeling domain are provided by the EPA AQS monitoring system (US EPA, 2013). These sites include measurements of $O_3$, CO, NO, $NO_2$, $NO_y$, $SO_2$, $PM_{2.5}$, $PM_{10}$, temperature, relative humidity, wind speed, and wind direction (not all sites contain all species at all times) and their locations are shown in Figure 2B-C. In addition, gas- and aerosol-phase measurements were collected concurrent to the modeling period in Pasadena at Caltech. The Caltech air quality system (CITAQS) measures $O_3$, CO, NO, $NO_2$, $NO_y$, $SO_2$, and $PM_{2.5}$ (Parker et al., 2020).

Measurements of $PM_1$ (fine PM with diameters less than 1 μm) and its components (organic, $NH_4$, $NO_3$, $SO_4$, and Cl) were performed using an Aerodyne high resolution time-of-flight aerosol mass spectrometer (HR-ToF-AMS) as described in Schulze et al. (submitted, 2022). Briefly, the AMS measures submicron, non-refractory $PM_1$ (NR-$PM_1$) at high time resolution. During the 2020 measurement campaign, the AMS isokinetically sampled air from a stainless-steel line downstream of a 2.5 μm cut diameter Teflon-coated cyclone mounted on the roof of the Linde Laboratory at Caltech. Approximately 6 m of stainless steel tubing connected the cyclone to the inlet of the HR-ToF-AMS. Standard methods were used to correct the data for gas-phase interferences and composition-dependent collection efficiencies (Middlebrook et al., 2012). Daily detection limits for aerosol chemical classes were calculated as three times the standard deviation of 30-minute blank measurements made with a high-efficiency particle arrestance (HEPA) filter. Daily detection limits for OA ranged from ~0.1-0.3 μg $m^{-3}$. The ionization efficiency of nitrate and relative ionization efficiency of ammonium were calibrated weekly using 350 nm ammonium nitrate particles size selected with a differential mobility analyzer.

Positive matrix factorization (PMF) was applied to the OA mass spectral datasets to gain insight into OA sources. PMF results presented here were taken from a larger analysis of data collected in 2020 (April 8 – July 19, 2020). A detailed description of PMF solution selection is provided in Schulze et al. (2022). A total of five factors, corresponding to less-oxidized oxygenated OA (LO-OOA), more-oxidized oxygenated OA (MO-OOA), hydrocarbon-like OA (HOA), cooking-influenced OA (CIOA), and an organic-nitrate influenced LO-OOA (LO-OOA-ON),

https://doi.org/10.5194/egusphere-2023-749
Preprint. Discussion started: 3 May 2023


were extracted from the OA dataset. Factors were identified using correlations with known tracers and comparisons of mass spectral and diurnal profiles to those extracted previously in Los Angeles (Hayes et al., 2013) and other urban areas (Hu et al., 2016; J. Xu et al., 2016). For comparisons with model predictions, we combine the HOA and CIOA factors as primary OA (POA), though we note that SOA formed from low-volatility species may appear spectrally similar to HOA (Lambe et al., 2012), as discussed in Schulze et al. (2022).

Multiple statistics are used to compare modeled data to observed data. These are mean bias (MB), normalized mean bias (NMB), root mean square error (RMSE), and $r^2$ (the square of the Pearson correlation coefficient), defined below. In these equations, $M$ is modeled data, $O$ is observed data, $\bar{M}$ is the mean of the modeled data, $\bar{O}$ is the mean of the observed data, and $N$ is the number of data points.

$$MB = \frac{1}{N}\sum_1^N (M - O) \quad (1)$$

$$Fractional\ NMB = \frac{\sum_1^N (M-O)}{\sum_1^N O} \quad (2)$$

$$NMB = \frac{\sum_1^N (M-O)}{\sum_1^N O} x100\% \quad (3)$$

$$RMSE = \sqrt{\frac{1}{N}\sum_1^N (M-O)^2} \quad (4)$$

$$r^2 = \frac{\left(\sum_1^N (M-\bar{M})(O-\bar{O})\right)^2}{\sum_1^N (M-\bar{M})^2 \sum_1^N (O-\bar{O})^2} \quad (5)$$

## 3. Results & Discussion

### 3.1 Evaluation of CTM Inputs

#### 3.1.1 Meteorology

The WRF predictions are compared to the AQS observations and the model performs very well in predicting temperature. The NMB values of temperature, relative humidity, wind speed, and wind direction at all AQS sites are calculated in the LA domain (Figure 5), and statistics are averaged using all site data in Table S1. Temperature is predicted well, with very low bias (NMB = 3.8%) and low scatter ($r^2$ = 0.97). Relative humidity is moderately well-predicted, with low scatter ($r^2$ = 0.81) but nonnegligible bias (NMB = -21.3%). Errors in relative humidity will affect the water content of aerosols and the resulting partitioning of aqueous aerosol, and the concentrations of other inorganic aerosol components like ammonium, nitrate, and chloride. Wind speed and direction tends not to be predicted well, with high bias and high scatter, but the error is highly variable between sites (Figure 5). Wind speed and direction error will potentially affect the transport between grid cells. The domain-wide statistics (Table S1) capture data over a long time period and over sites with different meteorology, so the error at individual sites must be investigated when making site-specific comparisons. Despite the range of sites contained in these statistics, temperature is well-predicted. This is critical, as temperature has a substantial impact on atmospheric chemistry and reaction rates.

https://doi.org/10.5194/egusphere-2023-749
Preprint. Discussion started: 3 May 2023


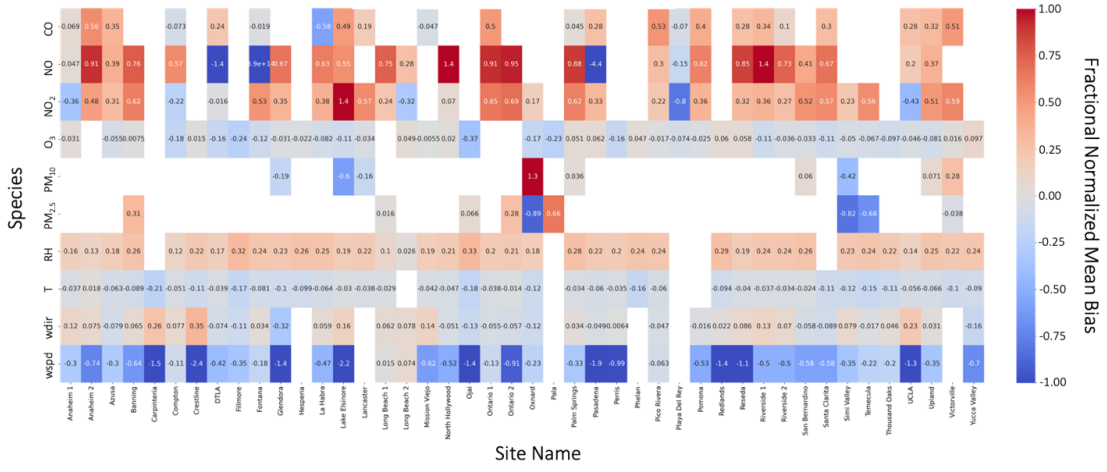


Figure 5: Fractional NMB of pollutants (rows) at all EPA AQS sites (columns) in the LA domain using daily-average values April 1–30, 2020. Empty boxes represent sites without measurements of the given pollutant.

### 3.1.2 Coarse-Resolution Simulation Results

California coarse-resolution CMAQ simulation results provide the lateral chemical boundary conditions for the inner LA domain. Predicted pollutant concentrations from the coarse-resolution California simulation are compared to EPA AQS monitoring site data in Table 1. $O_3$ is well-predicted based on its low MB, NMB, and RMSE. CO, $NO_x$, and $PM_{10}$ are all underpredicted (MB and NMB) with moderately high scatter (RMSE and $r^2$), while $PM_{2.5}$ is overpredicted. $SO_2$ is greatly overpredicted (MB and NMB). The accuracy of the region covering the Los Angeles Basin is of particular importance since that region will provide the initial and boundary conditions for the fine-resolution domain. Those results are compared to AQS measurements (Table 1) and demonstrate some different behaviors than the results of the full domain. $NO_x$ is slightly better predicted, while still underestimated, but $O_3$ is now underpredicted and less accurate. Average $PM_{2.5}$ mass increases substantially, as expected due to the higher air pollution in LA compared to other regions in California. $PM_{2.5}$ also becomes greatly overpredicted in the model (MB and NMB) and will be considered when evaluating the results of the fine-resolution simulation. The model bias remains approximately consistent for CO, $SO_2$, and $PM_{10}$.

https://doi.org/10.5194/egusphere-2023-749
Preprint. Discussion started: 3 May 2023


Table 1: Statistical analysis of daily-averaged CMAQ predictions for the (top) CA coarse-resolution domain and (bottom) LA Basin subset of the California domain, compared to EPA AQS monitoring site data.

| | $O_3$ | CO | $NO_x$ | $SO_2$ | $PM_{2.5}$ | $PM_{10}$ |
|---|---|---|---|---|---|---|
| **California Coarse-Resolution Simulation** | | | | | | |
| **Number of Data Points** | 341 | 248 | 310 | 62 | 186 | 93 |
| **Observed Mean** | 32.6 ppb | 221 ppb | 9.09 ppb | 0.095 ppb | 5.29 μg $m^{-3}$ | 17.0 μg $m^{-3}$ |
| **Modeled Mean** | 33.1 ppb | 140 ppb | 7.88 ppb | 0.217 ppb | 7.21 μg $m^{-3}$ | 12.1 μg $m^{-3}$ |
| **MB** | 0.44 ppb | -81 ppb | -1.20 ppb | 0.123 ppb | 1.92 μg $m^{-3}$ | -4.87 μg $m^{-3}$ |
| **NMB** | 1.36% | -36.5% | -13.2% | 129% | 36.3% | -28.7% |
| **RMSE** | 6.37 ppb | 99.2 ppb | 8.07 ppb | 0.160 ppb | 5.41 μg $m^{-3}$ | 10.5 μg $m^{-3}$ |
| **$r^2$** | 0.23 | 0.40 | 0.37 | 0.15 | 0.51 | 0.28 |
| **Los Angeles Subset of California Coarse-Resolution Simulation** | | | | | | |
| **Number of Data Points** | 126 | 134 | 155 | 31 | 36 | 33 |
| **Observed Mean** | 33.3 ppb | 242 ppb | 13.2 ppb | 0.090 ppb | 8.60 μg $m^{-3}$ | 21.2 μg $m^{-3}$ |
| **Modeled Mean** | 29.5 ppb | 170. ppb | 12.6 ppb | 0.223 ppb | 18.2 μg $m^{-3}$ | 15.5 μg $m^{-3}$ |
| **MB** | -3.77 ppb | -72.2 ppb | -0.62 ppb | 0.133 ppb | 9.65 μg $m^{-3}$ | -5.70 μg $m^{-3}$ |
| **NMB** | -11.3% | -29.8% | -4.72% | 147% | 112% | -26.8% |
| **RMSE** | 7.06 ppb | 85.0 ppb | 10.8 ppb | 0.17 ppb | 11.9 μg $m^{-3}$ | 8.36 μg $m^{-3}$ |
| **$r^2$** | 0.36 | 0.52 | 0.25 | 0.26 | 0.49 | 0.66 |

### 3.2 Evaluation of Fine-Resolution Model Predictions

Model predictions are compared to EPA AQS measurements at 44 sites in the domain (Figure 5-6, Table S2). $O_3$ has low NMB at all sites (NMB = 10.2%) despite high scatter ($r^2$ = 0.30), and has the correct spatial distribution despite poorly predicted $NO_x$. NO, $NO_2$, and CO prediction error can be positive or negative depending on location. PM measurements are limited in the domain and will be investigated further in Sections 3.3-3.4. Domain-wide statistics are provided in Table S2. $NO_x$ and VOC concentrations are highest in polluted and high-emitting regions, and O3 titration by freshly emitted NO results in $O_3$ concentrations that are lower in the

https://doi.org/10.5194/egusphere-2023-749
Preprint. Discussion started: 3 May 2023


urban core than in surrounding areas. Fine PM ($PM_1$ and $PM_{2.5}$) are highest in the urban center, while $PM_{10}$ concentrations increase over the ocean due to sea spray aerosol. Because of the potential overprediction of sea spray emissions, it is possible that $PM_{10}$ is overpredicted. POA is highest over high-emission regions, while SOA is highest over downwind regions, displaying the importance of chemical aging during transport.

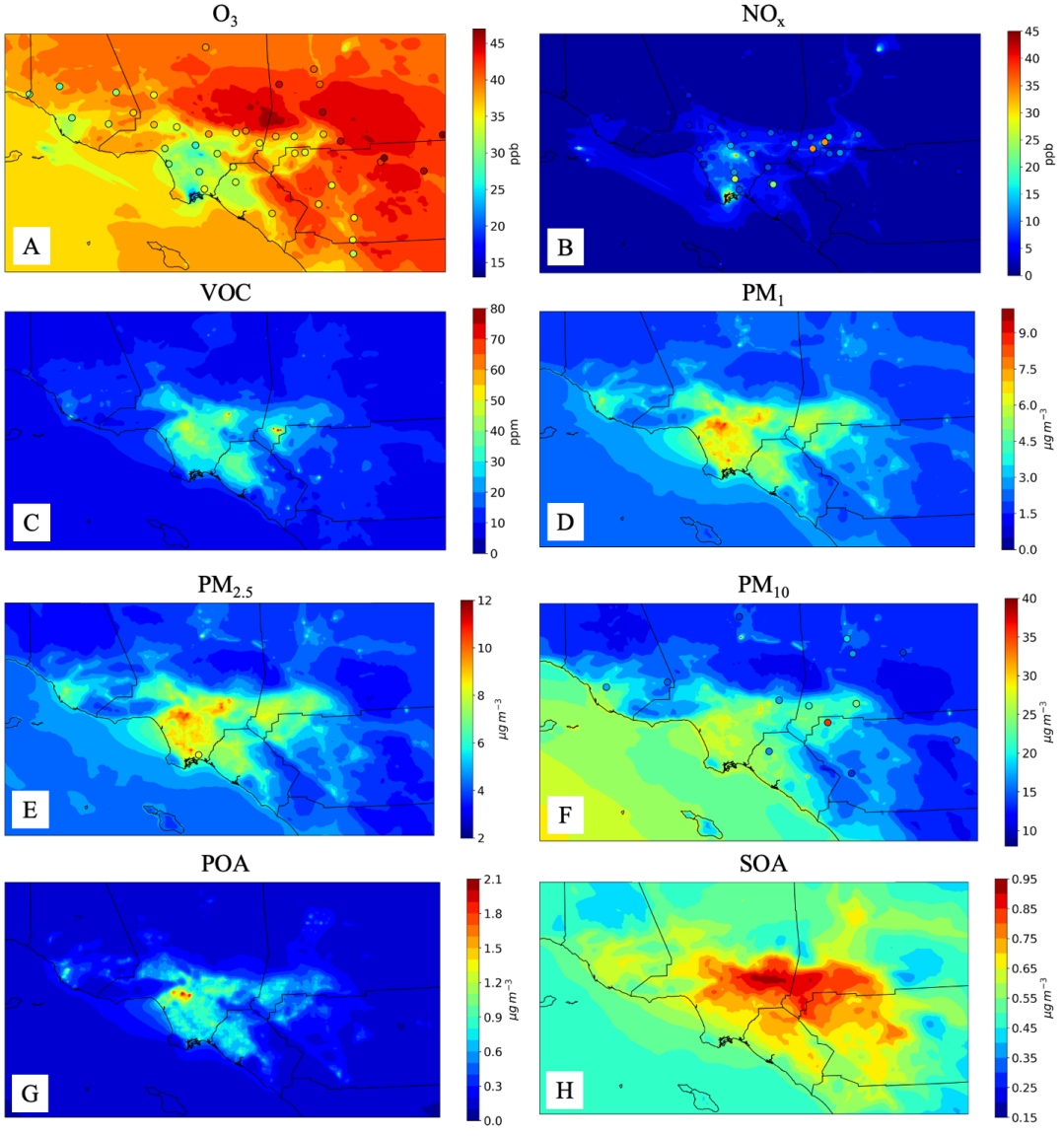


Figure 6: Time-averaged (April 1–30, 2020) CMAQ predicted concentration of A) $O_3$ (ppb), B) $NO_x$ (ppb), C) total VOC (ppm), D) $PM_1$ (μg $m^{-3}$), E) $PM_{2.5}$ (μg $m^{-3}$), F) $PM_{10}$ (μg $m^{-3}$), G) POA

https://doi.org/10.5194/egusphere-2023-749
Preprint. Discussion started: 3 May 2023


(μg $m^{-3}$), and H) SOA (μg $m^{-3}$). Circles depict the average concentration measured at the EPA AQS site at that location. There are no AQS measurements of VOCs, $PM_1$, POA, or SOA.

### 3.3 Evaluation of Aerosol Chemistry by Ground-Based Observations in Pasadena

Modeled $PM_1$ is underestimated due primarily to a large underestimation of OA. $PM_1$ mass and composition in Pasadena measured by AMS and predicted by CMAQ are compared in Figure 7. All predicted inorganic component ($SO_4$, $NO_3$, $NH_4$, Cl) concentrations are smaller by mass than observed values. Of note, $PM_1$ $NO_3$ is nearly well-predicted (Table S3) despite gaseous $NO_x$ underpredictions (Table S4). The model additionally predicts "other" inorganic $PM_1$, which includes EC, soil, and crustal elements which is not measured at the Pasadena ground site. The overall $PM_1$ bias (NMB = -49.1%) is caused by the large underprediction of OA (NMB = -63.0%). POA is well-predicted (Figure 8A) and the diurnal trend matches predictions except during late night and early morning hours (Figure 8B). SOA is significantly underpredicted (Figure 8A) and has an accurate diurnal trend except during early morning (Figure 8B). During the day when emissions and photochemistry are at maximum, measured and observed SOA peaks. SOA decreases in the evening as emissions decrease. Despite lower photochemistry and emissions, SOA (and other pollutant levels) remain high at night due to low planetary boundary layer (PBL) height.

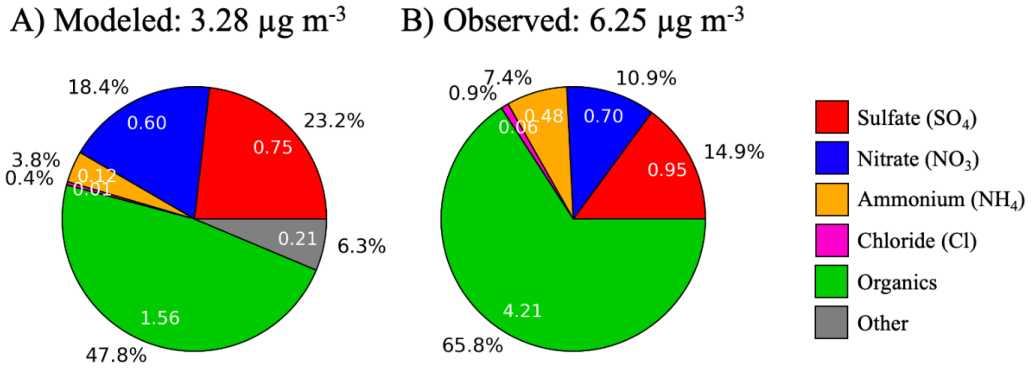


Figure 7: $PM_1$ composition averaged April 8–30, 2020 in Pasadena A) predicted by CMAQ and B) measured by AMS. Values inside the pie represent average mass values (μg $m^{-3}$) and values outside the pie represent the percentage of the total mass of each component.

Detailed model speciation and source apportionment can be used to understand the major sources of OA precursors in Pasadena and the error in SOA predictions. Measured POA comprises cooking-influenced OA (CIOA) and hydrocarbon-like OA (HOA). CIOA peaks overnight due to the PBL height dilution effect during the day, while HOA remains high throughout the day due to high local primary emissions sources (Figure 8). Measured SOA comprises more-oxidized oxygenated OA (MO_OOA), less-oxidized oxygenated OA (LO_OOA), and LO_OOA associated with organic nitrates (LO_OOA_ON). MO_OOA is consistently one of the largest OA components, with little diurnal variation. LO_OOA is the largest SOA component and has a sharp peak midday, consistent with higher oxidation rates during midday. Modeled alkane-like IVOCs have a similar high peak around midday, although of a smaller magnitude (Figure 8D). LO_OOA_ON have a small midday peak suggesting some photochemical production, but the largest contribution from LO_OOA_ON is overnight. This could be due in part to the PBL effect, and may also be due to overnight $NO_3$ chemistry producing organic nitrates. This is consistent

https://doi.org/10.5194/egusphere-2023-749
Preprint. Discussion started: 3 May 2023


with the overnight peak of modeled organic nitrates (Figure 8D) and terpene- and glyoxal-derived SOA (Figure S10), which are biogenic in nature. All other modeled SOA species except oligomers have low overnight mass and peak at midday, but their magnitudes are small which are likely a source of error in the CMAQ chemical mechanism. CMAQ lacks species which are behaving like LO-OOA, and the inclusion of additional SOA precursor species could improve SOA predictions (Pye et al., 2022). One potential source of error could be too-low yields of species that already exist in the model, such as aromatics, which have not been corrected for gas-phase wall losses (Zhang et al., 2014). Additional sources of error could include missing emissions, such as from asphalt which would peak during midday when temperatures are highest, consistent with LO-OOA.

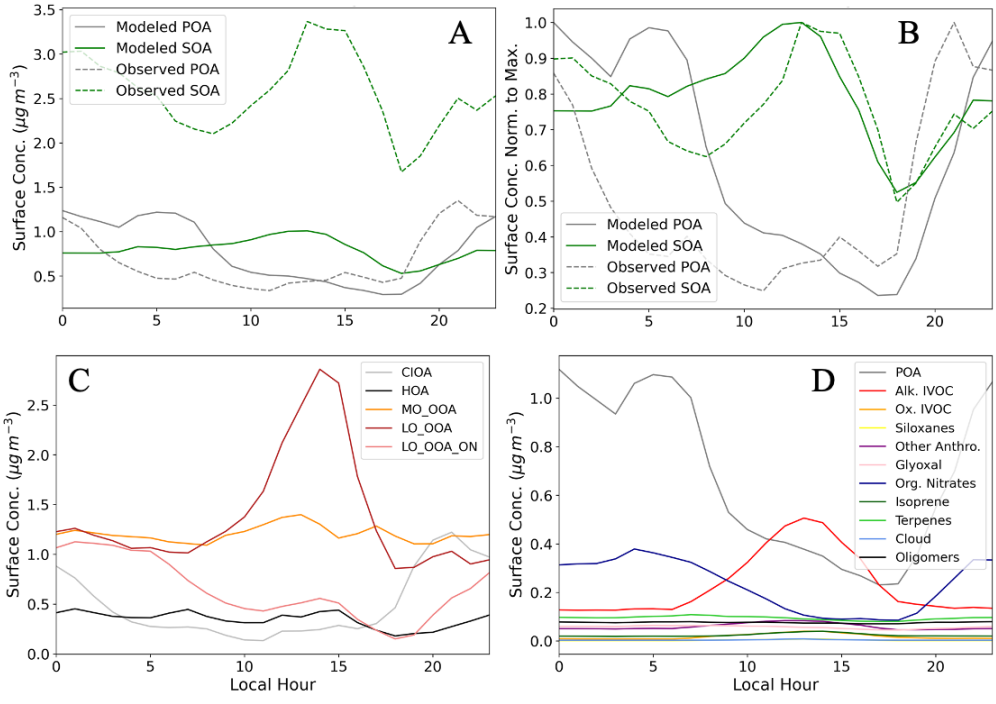


Figure 8: A) Modeled (solid) and measured (dashed) POA (gray) and SOA (green) diurnal variation in Pasadena. B) Modeled (solid) and measured (dashed) POA (gray) and SOA (green) diurnal variation in Pasadena. Surface concentration was normalized to the daily-maximum surface concentration. C) PMF-calculated POA and SOA speciation in Pasadena. D) Model-predicted POA and SOA speciation in Pasadena. All diurnal trends calculated April 8–30, 2020.

### 3.4 LA Basin Source Apportionment

The impact of removing each emission source on $O_3$ is presented in Figure 9 and these changes can be understood by investigating the changes in $NO_x$, VOC, and OH (Figures S12-14). The impact of sea spray is small because sea spray emits only particles, so those results are presented in Figure S11. $O_3$ decreased everywhere in response to the removal of VCP and biogenic emissions. VCPs only emit VOCs, and so the elimination of VCP emissions leads to VOC decreases everywhere. In response, OH and $NO_x$ concentrations increase, and the importance of

https://doi.org/10.5194/egusphere-2023-749
Preprint. Discussion started: 3 May 2023


transport and secondary aging processes is evident by the downwind location of most of the OH increase. The $O_3$ decrease resulting from VOC decreases is consistent with $NO_x$-saturated behavior, which has typically described highly-polluted urban areas. The removal of biogenic emissions has a similar response, as biogenic sources mainly emit VOCs. One exception lies in that biogenic sources also emit NO, so the VOC:$NO_x$ ratio changes less and thus biogenics have a smaller impact on $O_3$ change than VCPs do. In both cases of VCP and biogenic emissions removal, the outer regions display less sensitivity as a reduction in VOCs results in a near-zero change in $O_3$.

On-road vehicles and area+point sources emit $NO_x$, VOC, particles, and other inorganic gas-phase species. When these emission sources are removed, VOC and $NO_x$ concentrations decrease everywhere. In the urban core where VOC and $NO_x$ concentrations are high, OH and $O_3$ increase in response to the combined on-road VOC and $NO_x$ reductions. This is characteristic of the effect of large NOx relative to VOC (Figure 4) reductions under $NO_x$-saturated conditions. In contrast, the outer regions display behavior closer to $NO_x$-limited behavior, where VOC and $NO_x$ reductions result in OH and $O_3$ reductions. The reductions are small, suggesting that $O_3$ is not sensitive to emission reductions in these regions. The elimination of area+point source emissions has a similar impact on $O_3$. OH and $O_3$ increase in the urban core, with a decrease of OH and $O_3$ in the outer regions. The importance of ships and the Long Beach Port is evident, but it is likely that shipping emissions of $NO_x$ are overestimated relative to other area source emissions (Figure S8) and so this impact may be overstated in these results.

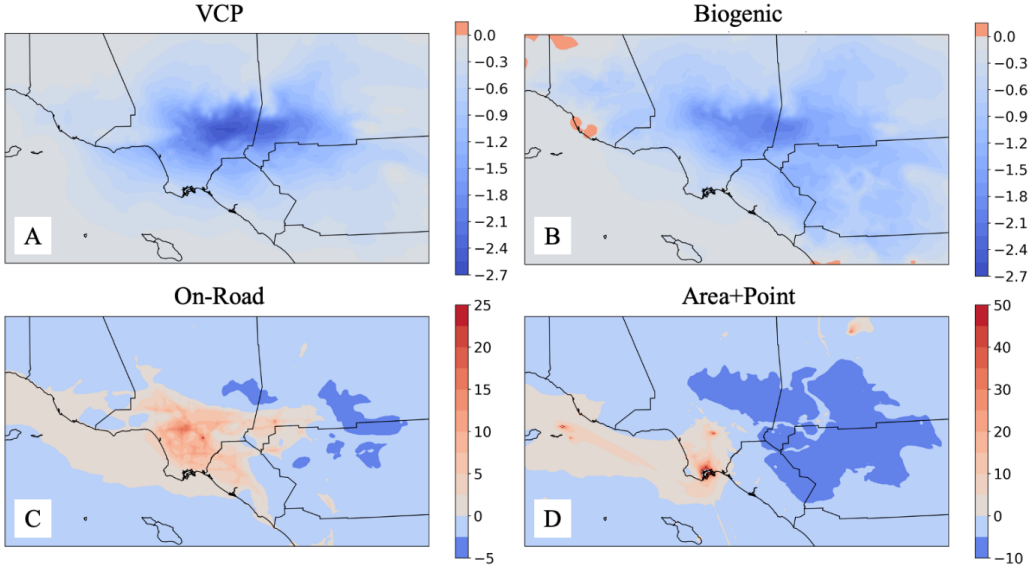


Figure 9: Percent change in average (April 1–30, 2020) predicted $O_3$ concentration averaged April 1–30, 2020 caused by removing each emission source: A) VCP, B) biogenic, C) on-road vehicles, and D) area+point.

$PM_{2.5}$ concentrations decrease everywhere in response to emission reductions (Figure 10). VCPs and biogenic sources emit only gas-phase species, so PM is formed exclusively via secondary processes. Biogenic PM is formed mostly over high emission areas like mountains, while VCP-derived PM is found in downwind regions, highlighting the importance of secondary

https://doi.org/10.5194/egusphere-2023-749
Preprint. Discussion started: 3 May 2023


formation during transport, similar to $O_3$ formation (Figure 9). PM from on-road and area+point sources is predominantly emitted directly because most of the impact to $PM_{2.5}$ is located in high emission regions. This is in spite of increased oxidation capacity in the high-emission regions (Figure S11). So if the emissions are removed entirely, as in this study, $PM_{2.5}$ will decrease. However, if the emissions were not entirely removed, the increased OH and the nonlinearity of atmospheric chemistry could lead to increased PM. Sea spray particles are reduced along the coastline where waves break (Figure S15).

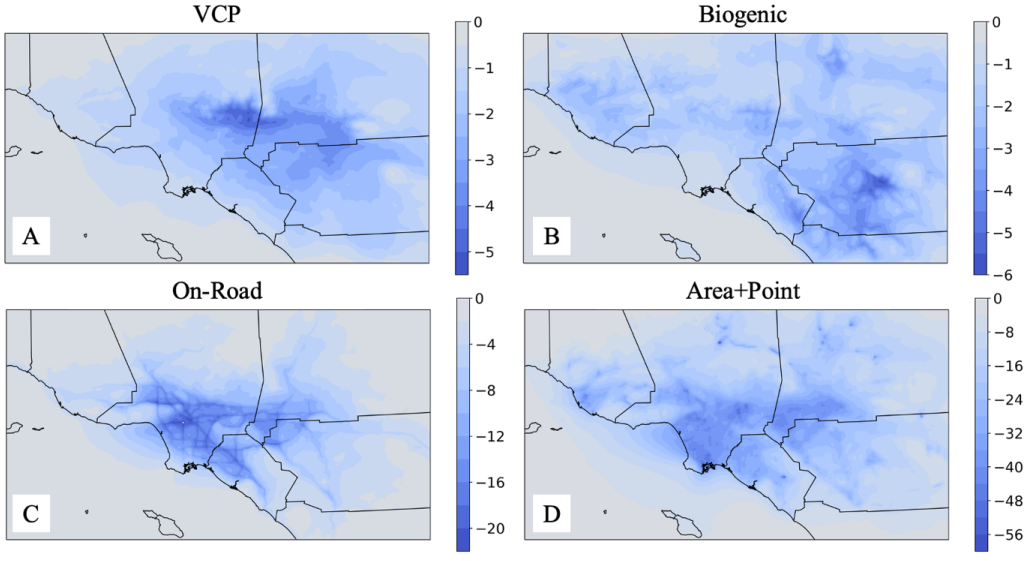


Figure 10: Percent change in average (April 1–30, 2020) predicted $PM_{2.5}$ concentration caused by removing each emission source: A) VCP, B) biogenic, C) on-road vehicles, and D) area+point.

Different species impact the $PM_{2.5}$ change from each emission source (Figure S16). On-road sources primarily decrease the $NO_3$ and $NH_4$ components of $PM_{2.5}$, both by direct emission and emissions of gas-phase $NO_x$. The reduction of on-road VOCs has relatively little impact on the organic fraction of $PM_{2.5}$. Area+point emissions also reduce $PM_{2.5}$ $NO_3$ and $NH_4$, plus other direct emissions like POA and elemental carbon (EC). VCPs and biogenic sources emit only VOCs, so they impact mostly the SOA fraction of $PM_{2.5}$. The reduction of VOCs leads to increases in OH and $NO_x$ and thus increases of $PM_{2.5}$ $NO_3$ and $NH_4$.

SOA decreases almost everywhere in response to the removal of emission sources but can increase in some high-emission regions (Figure 11). The SOA change from VCPs is downwind of the main emission regions. Biogenic SOA decrease is located mostly in remote, mountainous regions. Downwind SOA decreases when all on-road emissions are removed, but SOA in the downtown LA region increases. This occurs because it is $NO_x$-saturated and has increased OH concentrations (Figure S12), which increases rates of VOC oxidation and therefore SOA formation. The SOA decrease from the removal of area+point emission sources is more widely distributed than the emissions themselves (Figures S2-7), displaying the importance of SOA formation during transport.

https://doi.org/10.5194/egusphere-2023-749
Preprint. Discussion started: 3 May 2023


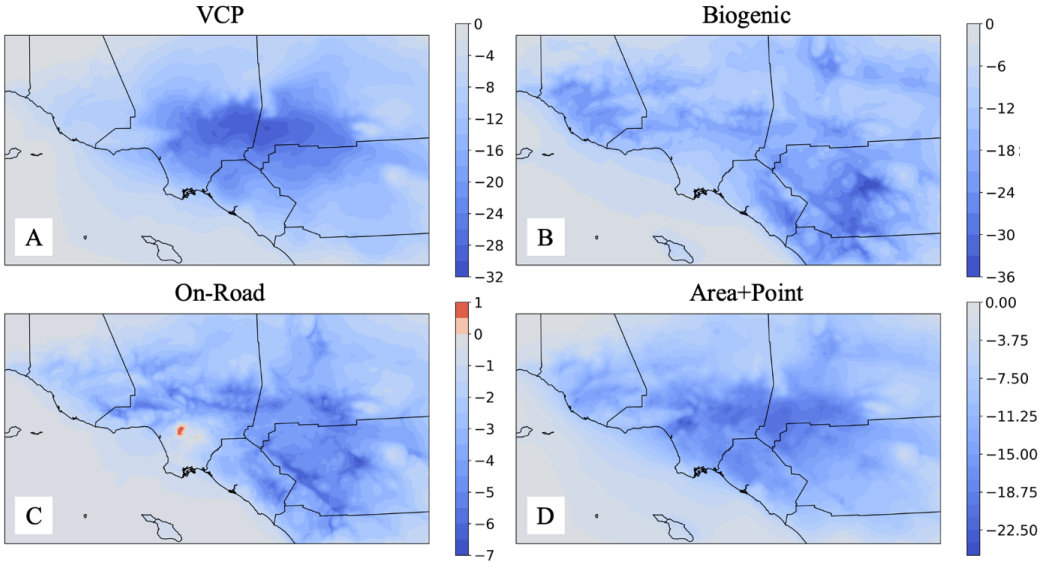


Figure 11: Percent change in average (April 1–30, 2020) predicted SOA concentration caused by removing each emission source: A) VCP, B) biogenic, C) on-road vehicles, and D) area+point.

SOA speciation varies throughout the domain and is dependent on location-specific emissions and meteorology (Figure S17). The largest components of SOA are derived from alkane-like IVOCs, organic nitrates, and monoterpenes. Alkane-like IVOC concentrations are highest downwind of high-emissions regions, demonstrating the importance of secondary formation during transport. Organic nitrate concentrations are highest over high-emission areas where VOC and $NO_x$ concentrations are largest. Monoterpene concentrations are more uniform and have both anthropogenic (i.e., VCP) and biogenic sources. Little SOA throughout the domain is formed from siloxanes, sesquiterpenes, or cloud processing. Biogenic SOA is primarily derived from sesquiterpenes, monoterpenes, and isoprene, and these aerosol species dominate over mountainous and remote areas in the outer regions of the domain.

SOA formation chemistry can be further understood by investigating the source apportionment of SOA components in Pasadena. The impact of removing each emission source on each modeled SOA component is given in

https://doi.org/10.5194/egusphere-2023-749
Preprint. Discussion started: 3 May 2023


*Table 2*. The main component of SOA—alkane-like IVOCs—originates particularly from VCPs and area+point emission sources. Alkane-like IVOCs are emitted from VCPs as low-volatility gases, while they are evaporated and oxidized POA from area+point emission sources. Organic nitrates have important contributions from VCPs and area+point emission sources, but are mostly formed from biogenic precursors. Despite VCP, biogenic, and area+point emission sources being highest during daytime, organic nitrates peak overnight due to nighttime $NO_3$ chemistry. In general, our modeling suggests SOA in LA is mostly driven by VCP, area, and point emission sources.

https://doi.org/10.5194/egusphere-2023-749
Preprint. Discussion started: 3 May 2023


Table 2: Mass concentration change (ng $m^{-3}$) of SOA components averaged over the LA domain when each emission source is removed.

| **ng $m^{-3}$** | VCP | Onroad | Biogenic | Sea Spray | Area+Point |
|---|---|---|---|---|---|
| Alkane-like IVOCs | -36.03 | -4.89 | 1.29 | -0.01 | -23.76 |
| Oxygenated IVOCs | -4.61 | -0.17 | 0.03 | 0.002 | -0.38 |
| Siloxanes | -1.10 | -0.09 | 0.006 | $-7.3 \times 10^{-4}$ | -0.27 |
| Glyoxal | -1.01 | -1.05 | -2.11 | -0.10 | -2.88 |
| Other anthropogenic | -3.69 | -0.71 | -1.10 | 0.07 | -2.63 |
| Isoprene | -0.41 | -0.29 | -5.24 | $6.7 \times 10^{-4}$ | -1.03 |
| Monoterpenes | -2.41 | 0.56 | -18.36 | -0.01 | -1.40 |
| Sesquiterpenes | -0.13 | -0.05 | -0.15 | $-3.4 \times 10^{-4}$ | -0.24 |
| Organic nitrates | -10.52 | -5.64 | -42.53 | 0.14 | -16.08 |
| Oligomers | -0.83 | -0.30 | -1.35 | $7.9 \times 10^{-4}$ | -0.90 |
| Cloud-processed | -0.10 | -0.10 | -0.15 | $-1.8 \times 10^{-4}$ | -0.26 |

## 4. Conclusions

This study presents a new model framework to simulate air quality in Los Angeles. Past modeling studies of LA focus on 2010 to overlap with the CalNex campaign, and few exist which focus on SOA sources and speciation. We developed state-of-the-science inputs of meteorology, emissions, and boundary conditions, and show that these inputs are comparable to observations. Emissions are separated into 3 anthropogenic categories—VCP, on-road, and area+point—and 2 natural categories—gases and sea spray—allowing for source apportionment studies.

The model is set up for April 2020 and the results are compared to observations, aiming to better understand the chemistry leading to pollutant formation. Temperature and $O_3$ are very well-predicted, but $NO_x$ and PM are underpredicted. In particular, OA is underpredicted in Pasadena when compared to AMS measurements. While POA is well-predicted, SOA is greatly under-predicted. The main components of modeled SOA are alkane-like IVOCs and organic nitrates, while other categories of SOA are likely underpredicted; for example, oxygenated IVOCs which have not been well-classified in laboratory settings.

This study stresses that improved model predictions will require updated chemistry and emissions. The chemistry of SVOCs is not well-understood, and better representations should be included in CMAQ as they are developed. SVOCs are also typically not represented in emission inventories, and while the VCP inventory used here utilizes new SVOC speciation profiles, the other categories of emissions did not specifically study SVOCs. The chemistry of oxygenated species has not been extensively studied, and should be focused on in future work due to the prevalence of oxygenated emissions and atmospheric constituents (Pennington et al., 2021). Some emissions from anthropogenic sources are likely underpredicted. For example, boats are estimated to emit more $NO_x$ than off-road sources, but off-road sources should likely be the main area source of $NO_x$ (Khare & Gentner, 2018). Also, many forms of asphalt emissions are not included in VCP or area sources, but likely will contribute significant SOA and therefore reduce modeled SOA bias (Khare & Gentner, 2018).

https://doi.org/10.5194/egusphere-2023-749
Preprint. Discussion started: 3 May 2023


The source apportionment results convey important qualities about the VOC-$NO_x$ regime of the LA atmosphere. The urban core of LA demonstrates $NO_x$-saturated behavior: $NO_x$ reductions lead to $O_3$ increase, while VOC reductions lead to $O_3$ decrease. Outside of the urban core, $O_3$ decreases in response to any level of either $NO_x$ or VOC removal, suggesting a regime that is less $NO_x$-saturated than the urban region, such as a regime lying close to the $O_3$-$NO_x$-VOC ridgeline in the VOC-sensitive regime (Seinfeld & Pandis, 2016). Reducing $O_3$ is a consistent goal for policymakers, and this work shows that $O_3$ in Los Angeles is reduced by the removal of VOCs. $NO_x$ emission decreases remain important, as these decreases will move the Basin from a $NO_x$-saturated regime closer to a $NO_x$-sensitive regime. However, $NO_x$ reductions without concurrent or larger reductions in VOC concentrations will make $O_3$ pollution worse until the $NO_x$-sensitive regime is reached. It is also important to consider the spatial distribution of emissions and reduction policies. Reducing $NO_x$ and/or VOC emissions in the outer regions of the domain will have a lesser impact than reductions in the urban core, or may have an opposite effect, as demonstrated in this study. The increased oxidative capacity of the $NO_x$-saturated regions also has an impact on SOA formation and the formation of secondary inorganic components of PM. Focusing on emissions in the urban core is critical and will affect downwind regions. It should be noted that this study was performed in the spring season, which is not peak ozone season. Thus, results may differ in the summer months and further studies should investigate this period.

In Part 2 (Pennington et al., in prep), the new model framework is used to investigate future emission scenarios involving VCP and on-road vehicle emissions during the 2020 lockdown of the pandemic. VCP emissions have been quantified in multiple studies (i.e., Seltzer, Pennington, et al., 2021; McDonald et al., 2018), but none of these studies have investigated the implications of future VCP emissions. We reduce VCP emissions to investigate the impact on $O_3$, $NO_x$, PM, and SOA speciation. Additionally, we run the model in a "non-COVID" scenario, where on-road emissions are represented without COVID-induced VMT reductions. In this way, the impact of emissions versus meteorology on 2020 air quality can be distinguished. Understanding these possible outcomes can shape informed policy decisions.

## Data Availability

These will be posted on Caltech's permanent data site.

- CMAQ source code
- WRF namelist files
- CA4km emission file
- All LA1km emission files (VCP, LDV, HDV, area, point)
- We'll add a README file which says that CMAQ and WRF output are available upon request

## Author Contributions

EAP, YW, and JHS designed and led the research project. EAP performed all model simulations, analyzed the data, and drafted the paper. BCS collected AMS data and performed PMF analysis. KMS provided VCP emissions. JY provided VMT data. ZJ and BZ provided emissions for the California 4 km x 4 km domain. MV provided the CARB emissions inventory and all SMOKE input files. DC provided the EMFAC emissions inventory. BNM and HOTP participated in useful research discussions and mentored EAP. CMK and RXW collected AMS data. All authors participated in useful research discussions and revised the paper.

https://doi.org/10.5194/egusphere-2023-749
Preprint. Discussion started: 3 May 2023


## Disclaimer

The views expressed in this article are those of the authors and do not necessarily represent the views or policies of the U.S. Environmental Protection Agency.

## Acknowledgements

The authors would like to thank Leonardo Ramirez for his guidance on the CARB emission inventories, and Han Kim for introducing and explaining useful Python analysis tools. We're also grateful to John Crounse and Harrison Parker for managing the CITAQS station and collecting the CITAQS data used in this study. EAP and JHS acknowledge funding support from Samsung Global Research Outreach Program. YW and JHS acknowledge funding support from the National Science Foundation (AGS-2103714). We also acknowledge high-performance computing support from NASA Pleiades.

## Competing interests

YW is a member of the editorial board of Atmospheric Chemistry and Physics.

https://doi.org/10.5194/egusphere-2023-749
Preprint. Discussion started: 3 May 2023


## References

Alapaty, K., Niyogi, D., Chen, F., Pyle, P., Chandrasekar, A., & Seaman, N. (2008). Development of the Flux-Adjusting Surface Data Assimilation System for Mesoscale Models. *Journal of Applied Meteorology and Climatology*, *47*(9), 2331–2350. https://doi.org/10.1175/2008JAMC1831.1

Appel, K. W., Bash, J. O., Fahey, K. M., Foley, K. M., Gilliam, R. C., Hogrefe, C., Hutzell, W. T., Kang, D., Mathur, R., Murphy, B. N., Napelenok, S. L., Nolte, C. G., Pleim, J. E., Pouliot, G. A., Pye, H. O. T., Ran, L., Roselle, S. J., Sarwar, G., Schwede, D. B., … Wong, D. C. (2021). The Community Multiscale Air Quality (CMAQ) model versions 5.3 and 5.3.1: System updates and evaluation. *Geoscientific Model Development*, *14*(5), 2867–2897. https://doi.org/10.5194/gmd-14-2867-2021

Bahreini, R., Middlebrook, A. M., Gouw, J. A. de, Warneke, C., Trainer, M., Brock, C. A., Stark, H., Brown, S. S., Dube, W. P., Gilman, J. B., Hall, K., Holloway, J. S., Kuster, W. C., Perring, A. E., Prevot, A. S. H., Schwarz, J. P., Spackman, J. R., Szidat, S., Wagner, N. L., … Parrish, D. D. (2012). Gasoline emissions dominate over diesel in formation of secondary organic aerosol mass. *Geophysical Research Letters*, *39*(6). https://doi.org/10.1029/2011GL050718

Bash, J. O., Baker, K. R., & Beaver, M. R. (2016). Evaluation of improved land use and canopy representation in BEIS v3.61 with biogenic VOC measurements in California. *Geoscientific Model Development*, *9*(6), 2191–2207. https://doi.org/10.5194/gmd-9-2191-2016

Binkowski, F. S., & Roselle, S. J. (2003). Models-3 Community Multiscale Air Quality (CMAQ) model aerosol component 1. Model description. *Journal of Geophysical Research: Atmospheres*, *108*(D6). https://doi.org/10.1029/2001JD001409

California Air Resources Board. (2018). *EMFAC2017 Volume III Technical Documentation: V1.0.2*. https://ww3.arb.ca.gov/msei/downloads/emfac2017-volume-iii-technical-documentation.pdf

Caltrans. (2020). *Caltrans PeMS*. https://pems.dot.ca.gov/

CARB. (2020). *Criteria Pollutant Emission Inventory Data | California Air Resources Board*. https://ww2.arb.ca.gov/criteria-pollutant-emission-inventory-data

Carlton, A. G., Bhave, P. V., Napelenok, S. L., Edney, E. O., Sarwar, G., Pinder, R. W., Pouliot, G. A., & Houyoux, M. (2010). Model Representation of Secondary Organic Aerosol in CMAQv4.7. *Environmental Science & Technology*, *44*(22), 8553–8560. https://doi.org/10.1021/es100636q

Carter, W. P. L. (2010). Development of the SAPRC-07 chemical mechanism. *Atmospheric Environment*, *44*(40), 5324–5335. https://doi.org/10.1016/j.atmosenv.2010.01.026

CMAS. (2020). *SMOKE (Sparse Matrix Operator Kerner Emissions) Modeling System*. CMAS: Community Modeling and Analysis System. https://www.cmascenter.org/smoke/index.cfm

Donahue, N. M., Epstein, S. A., Pandis, S. N., & Robinson, A. L. (2011). A two-dimensional volatility basis set: 1. organic-aerosol mixing thermodynamics. *Atmospheric Chemistry and Physics*, *11*(7), 3303–3318. https://doi.org/10.5194/acp-11-3303-2011

Ensberg, J. J., Hayes, P. L., Jimenez, J. L., Gilman, J. B., Kuster, W. C., de Gouw, J. A., Holloway, J. S., Gordon, T. D., Jathar, S., Robinson, A. L., & Seinfeld, J. H. (2014). Emission factor ratios, SOA mass yields, and the impact of vehicular emissions on SOA formation.

https://doi.org/10.5194/egusphere-2023-749
Preprint. Discussion started: 3 May 2023


*Atmospheric Chemistry and Physics*, *14*(5), 2383–2397. https://doi.org/10.5194/acp-14-2383-2014

Fountoukis, C., & Nenes, A. (2007). ISORROPIA II: A computationally efficient thermodynamic equilibrium model for $K^+$–$Ca^{2+}$–$Mg^{2+}$–$NH_4^+$–$Na^+$–$SO_4^{2-}$–$NO_3^-$–$Cl^-$–$H_2O$ aerosols. *Atmospheric Chemistry and Physics*, *7*(17), 4639–4659. https://doi.org/10.5194/acp-7-4639-2007

Gentner, D. R., Jathar, S. H., Gordon, T. D., Bahreini, R., Day, D. A., El Haddad, I., Hayes, P. L., Pieber, S. M., Platt, S. M., de Gouw, J., Goldstein, A. H., Harley, R. A., Jimenez, J. L., Prévôt, A. S. H., & Robinson, A. L. (2017). Review of Urban Secondary Organic Aerosol Formation from Gasoline and Diesel Motor Vehicle Emissions. *Environmental Science & Technology*, *51*(3), 1074–1093. https://doi.org/10.1021/acs.est.6b04509

Goliff, W. S., Stockwell, W. R., & Lawson, C. V. (2013). The regional atmospheric chemistry mechanism, version 2. *Atmospheric Environment*, *68*, 174–185. https://doi.org/10.1016/j.atmosenv.2012.11.038

Hayes, P. L., Ortega, A. M., Cubison, M. J., Froyd, K. D., Zhao, Y., Cliff, S. S., Hu, W. W., Toohey, D. W., Flynn, J. H., Lefer, B. L., Grossberg, N., Alvarez, S., Rappenglück, B., Taylor, J. W., Allan, J. D., Holloway, J. S., Gilman, J. B., Kuster, W. C., Gouw, J. A. de, … Jimenez, J. L. (2013). Organic aerosol composition and sources in Pasadena, California, during the 2010 CalNex campaign. *Journal of Geophysical Research: Atmospheres*, *118*(16), 9233–9257. https://doi.org/10.1002/jgrd.50530

Hersbach, H., Bell, B., Berrisford, P., Biavati, G., Horányi, A., Muñoz Sabater, J., Nicolas, J., Peubey, C., Radu, R., Rozum, I., Schepers, D., Simmons, A., Soci, C., Dee, D., & Thépaut, J.-N. (2018). *ERA5 hourly data on pressure levels from 1979 to present*. Copernicus Climate Change Service (C3S) Climate Data Store (CDS). 10.24381/cds.bd0915c6

Hogrefe, C., Gilliam, R., Mathur, R., Henderson, B. H., Sarwar, G., Appel, K. W., Pouliot, G., Willison, J., Miller, R., Vukovich, J., Eyth, A., Talgo, K., Allen, C., & Foley, K. (2021). *CMAQv5.3.2 ozone simulations over the Northern Hemisphere: Model performance and sensitivity to model configuration*. 20th Annual CMAS Conference. https://drive.google.com/drive/folders/1A1ZzJE1t7OgwSezQNvy3rt9aATnXA0k2

Hu, W., Hu, M., Hu, W., Jimenez, J. L., Yuan, B., Chen, W., Wang, M., Wu, Y., Chen, C., Wang, Z., Peng, J., Zeng, L., & Shao, M. (2016). Chemical composition, sources, and aging process of submicron aerosols in Beijing: Contrast between summer and winter. *Journal of Geophysical Research: Atmospheres*, *121*(4), 1955–1977. https://doi.org/10.1002/2015JD024020

Hyslop, N. P. (2009). Impaired visibility: The air pollution people see. *Atmospheric Environment*, *43*(1), 182–195. https://doi.org/10.1016/j.atmosenv.2008.09.067

Intergovernmental Panel on Climate Change (Ed.). (2014). Anthropogenic and Natural Radiative Forcing. In *Climate Change 2013 – The Physical Science Basis: Working Group I Contribution to the Fifth Assessment Report of the Intergovernmental Panel on Climate Change* (pp. 659–740). Cambridge University Press. https://doi.org/10.1017/CBO9781107415324.018

Jiang, Z., Shi, H., Zhao, B., Gu, Y., Zhu, Y., Miyazaki, K., Lu, X., Zhang, Y., Bowman, K. W., Sekiya, T., & Liou, K.-N. (2021). Modeling the impact of COVID-19 on air quality in southern California: Implications for future control policies. *Atmospheric Chemistry and Physics*, *21*(11), 8693–8708. https://doi.org/10.5194/acp-21-8693-2021

https://doi.org/10.5194/egusphere-2023-749
Preprint. Discussion started: 3 May 2023


Jimenez, J. L., Canagaratna, M. R., Donahue, N. M., Prevot, A. S. H., Zhang, Q., Kroll, J. H., DeCarlo, P. F., Allan, J. D., Coe, H., Ng, N. L., Aiken, A. C., Docherty, K. S., Ulbrich, I. M., Grieshop, A. P., Robinson, A. L., Duplissy, J., Smith, J. D., Wilson, K. R., Lanz, V. A., … Worsnop, D. R. (2009). Evolution of Organic Aerosols in the Atmosphere. *Science*, *326*(5959), 1525–1529. https://doi.org/10.1126/science.1180353

Keller, C. A., & Evans, M. J. (2019). Application of random forest regression to the calculation of gas-phase chemistry within the GEOS-Chem chemistry model v10. *Geoscientific Model Development Discussions*, 1209–1225.

Khare, P., & Gentner, D. R. (2018). Considering the future of anthropogenic gas-phase organic compound emissions and the increasing influence of non-combustion sources on urban air quality. *Atmospheric Chemistry and Physics*, *18*(8), 5391–5413. https://doi.org/10.5194/acp-18-5391-2018

Khare, P., Machesky, J., Soto, R., He, M., Presto, A. A., & Gentner, D. R. (2020). Asphalt-related emissions are a major missing nontraditional source of secondary organic aerosol precursors. *Science Advances*, *6*(36), eabb9785. https://doi.org/10.1126/sciadv.abb9785

Lambe, A. T., Onasch, T. B., Croasdale, D. R., Wright, J. P., Martin, A. T., Franklin, J. P., Massoli, P., Kroll, J. H., Canagaratna, M. R., Brune, W. H., Worsnop, D. R., & Davidovits, P. (2012). Transitions from Functionalization to Fragmentation Reactions of Laboratory Secondary Organic Aerosol (SOA) Generated from the OH Oxidation of Alkane Precursors. *Environmental Science & Technology*, *46*(10), 5430–5437. https://doi.org/10.1021/es300274t

Le, T., Wang, Y., Liu, L., Yang, J., Yung, Y. L., Li, G., & Seinfeld, J. H. (2020). Unexpected air pollution with marked emission reductions during the COVID-19 outbreak in China. *Science*, *369*(6504), 702–706. https://doi.org/10.1126/science.abb7431

Lim, S. S., Vos, T., Flaxman, A. D., Danaei, G., Shibuya, K., Adair-Rohani, H., AlMazroa, M. A., Amann, M., Anderson, H. R., Andrews, K. G., Aryee, M., Atkinson, C., Bacchus, L. J., Bahalim, A. N., Balakrishnan, K., Balmes, J., Barker-Collo, S., Baxter, A., Bell, M. L., … Ezzati, M. (2012). A comparative risk assessment of burden of disease and injury attributable to 67 risk factors and risk factor clusters in 21 regions, 1990–2010: A systematic analysis for the Global Burden of Disease Study 2010. *The Lancet*, *380*(9859), 2224–2260. https://doi.org/10.1016/S0140-6736(12)61766-8

Lu, Q., Murphy, B. N., Qin, M., Adams, P. J., Zhao, Y., Pye, H. O. T., Efstathiou, C., Allen, C., & Robinson, A. L. (2020). Simulation of organic aerosol formation during the CalNex study: Updated mobile emissions and secondary organic aerosol parameterization for intermediate-volatility organic compounds. *Atmospheric Chemistry and Physics*, *20*(7), 4313–4332. https://doi.org/10.5194/acp-20-4313-2020

McDonald, B. C., Gouw, J. A. de, Gilman, J. B., Jathar, S. H., Akherati, A., Cappa, C. D., Jimenez, J. L., Lee-Taylor, J., Hayes, P. L., McKeen, S. A., Cui, Y. Y., Kim, S.-W., Gentner, D. R., Isaacman-VanWertz, G., Goldstein, A. H., Harley, R. A., Frost, G. J., Roberts, J. M., Ryerson, T. B., & Trainer, M. (2018). Volatile chemical products emerging as largest petrochemical source of urban organic emissions. *Science*, *359*(6377), 760–764. https://doi.org/10.1126/science.aaq0524

Middlebrook, A. M., Bahreini, R., Jimenez, J. L., & Canagaratna, M. R. (2012). Evaluation of Composition-Dependent Collection Efficiencies for the Aerodyne Aerosol Mass Spectrometer using Field Data. *Aerosol Science and Technology*, *46*(3), 258–271. https://doi.org/10.1080/02786826.2011.620041

https://doi.org/10.5194/egusphere-2023-749
Preprint. Discussion started: 3 May 2023


Murphy, B. N., Nolte, C. G., Sidi, F., Bash, J. O., Appel, K. W., Jang, C., Kang, D., Kelly, J., Mathur, R., Napelenok, S., Pouliot, G., & Pye, H. O. T. (2021). The Detailed Emissions Scaling, Isolation, and Diagnostic (DESID) module in the Community Multiscale Air Quality (CMAQ) modeling system version 5.3.2. *Geoscientific Model Development*, *14*(6), 3407–3420. https://doi.org/10.5194/gmd-14-3407-2021

Murphy, B. N., Woody, M. C., Jimenez, J. L., Carlton, A. M. G., Hayes, P. L., Liu, S., Ng, N. L., Russell, L. M., Setyan, A., Xu, L., Young, J., Zaveri, R. A., Zhang, Q., & Pye, H. O. T. (2017). Semivolatile POA and parameterized total combustion SOA in CMAQv5.2: Impacts on source strength and partitioning. *Atmospheric Chemistry and Physics*, *17*(18), 11107–11133. https://doi.org/10.5194/acp-17-11107-2017

Nuvolone, D., Petri, D., & Voller, F. (2018). The effects of ozone on human health. *Environmental Science and Pollution Research*, *25*(9), 8074–8088. https://doi.org/10.1007/s11356-017-9239-3

Odum, J. R., Hoffmann, T., Bowman, F., Collins, D., Flagan, R. C., & Seinfeld, J. H. (1996). Gas/Particle Partitioning and Secondary Organic Aerosol Yields. *Environmental Science & Technology*, *30*(8), 2580–2585. https://doi.org/10.1021/es950943+

Parker, H. A., Hasheminassab, S., Crounse, J. D., Roehl, C. M., & Wennberg, P. O. (2020). Impacts of Traffic Reductions Associated With COVID-19 on Southern California Air Quality. *Geophysical Research Letters*, *47*(23), e2020GL090164. https://doi.org/10.1029/2020GL090164

Pennington, E. A., Seltzer, K. M., Murphy, B. N., Qin, M., Seinfeld, J. H., & Pye, H. O. T. (2021). Modeling secondary organic aerosol formation from volatile chemical products. *Atmospheric Chemistry and Physics*, *21*(24), 18247–18261. https://doi.org/10.5194/acp-21-18247-2021

Pleim, J. E. (2007). A Combined Local and Nonlocal Closure Model for the Atmospheric Boundary Layer. Part I: Model Description and Testing. *Journal of Applied Meteorology and Climatology*, *46*(9), 1383–1395. https://doi.org/10.1175/JAM2539.1

Pleim, J., & Ran, L. (2011). Surface Flux Modeling for Air Quality Applications. *Atmosphere*, *2*(3), Article 3. https://doi.org/10.3390/atmos2030271

Pye, H. O. T., Murphy, B. N., Xu, L., Ng, N. L., Carlton, A. G., Guo, H., Weber, R., Vasilakos, P., Appel, K. W., Budisulistiorini, S. H., Surratt, J. D., Nenes, A., Hu, W., Jimenez, J. L., Isaacman-VanWertz, G., Misztal, P. K., & Goldstein, A. H. (2017). On the implications of aerosol liquid water and phase separation for organic aerosol mass. *Atmospheric Chemistry and Physics*, *17*(1), 343–369. https://doi.org/10.5194/acp-17-343-2017

Pye, H. O. T., Pinder, R. W., Piletic, I. R., Xie, Y., Capps, S. L., Lin, Y.-H., Surratt, J. D., Zhang, Z., Gold, A., Luecken, D. J., Hutzell, W. T., Jaoui, M., Offenberg, J. H., Kleindienst, T. E., Lewandowski, M., & Edney, E. O. (2013). Epoxide Pathways Improve Model Predictions of Isoprene Markers and Reveal Key Role of Acidity in Aerosol Formation. *Environmental Science & Technology*, *47*(19), 11056–11064. https://doi.org/10.1021/es402106h

Pye, H. O. T., Place, B. K., Murphy, B. N., Seltzer, K. M., D'Ambro, E. L., Allen, C., Piletic, I. R., Farrell, S., Schwantes, R. H., Coggon, M. M., Saunders, E., Xu, L., Sarwar, G., Hutzell, W. T., Foley, K. M., Pouliot, G., Bash, J., & Stockwell, W. R. (2022). Linking gas, particulate, and toxic endpoints to air emissions in the Community Regional Atmospheric Chemistry Multiphase Mechanism (CRACMM) version 1.0. *Atmospheric Chemistry and Physics Discussions*, 1–88. https://doi.org/10.5194/acp-2022-695

https://doi.org/10.5194/egusphere-2023-749
Preprint. Discussion started: 3 May 2023


Qin, M., Murphy, B. N., Isaacs, K. K., McDonald, B. C., Lu, Q., McKeen, S. A., Koval, L., Robinson, A. L., Efstathiou, C., Allen, C., & Pye, H. O. T. (2021). Criteria pollutant impacts of volatile chemical products informed by near-field modelling. *Nature Sustainability*, *4*(2), Article 2. https://doi.org/10.1038/s41893-020-00614-1

Ritchie, S., & Tok, Y. C. (2016). *Development of a New Methodology to Characterize Truck Body Types Along California Freeways* (No. 11–316; p. 176). California Air Resources Board. https://ww2.arb.ca.gov/sites/default/files/classic/research/apr/past/11-316.pdf

Robinson, A. L., Donahue, N. M., Shrivastava, M. K., Weitkamp, E. A., Sage, A. M., Grieshop, A. P., Lane, T. E., Pierce, J. R., & Pandis, S. N. (2007). Rethinking Organic Aerosols: Semivolatile Emissions and Photochemical Aging. *Science*, *315*(5816), 1259–1262. https://doi.org/10.1126/science.1133061

Sandermann Jr, H. (1996). Ozone and Plant Health. *Annual Review of Phytopathology*, *34*(1), 347–366. https://doi.org/10.1146/annurev.phyto.34.1.347

Seinfeld, J. H., & Pandis, S. N. (2016). *Atmospheric Chemistry and Physics: From Air Pollution to Climate Change* (3rd ed.). John Wiley & Sons, Inc.

Seltzer, K. M., Murphy, B. N., Pennington, E. A., Allen, C., Talgo, K., & Pye, H. O. T. (2022). Volatile Chemical Product Enhancements to Criteria Pollutants in the United States. *Environmental Science & Technology*. https://doi.org/10.1021/acs.est.1c04298

Seltzer, K. M., Pennington, E., Rao, V., Murphy, B. N., Strum, M., Isaacs, K. K., & Pye, H. O. T. (2021). Reactive organic carbon emissions from volatile chemical products. *Atmospheric Chemistry and Physics*, *21*(6), 5079–5100. https://doi.org/10.5194/acp-21-5079-2021

Skamarock, W. C., Klemp, J. B., Dudhia, J., Gill, D. O., & Barker, D. (2008). *A Description of the Advanced Research WRF Version 3* (NCAR/TN-475+STR). University Corporation for Atmospheric Research. http://dx.doi.org/10.5065/D68S4MVH

US EPA. (2020). *CMAQ*. Zenodo. https://doi.org/10.5281/zenodo.4081737

US EPA. (2022). *Spatial Allocator v4.4 (June 2019 release)* [C++]. CMAS Center. https://github.com/CMASCenter/Spatial-Allocator/blob/14176784e03f7379d8c6a25f4ce7cfb2dd08128c/docs/User_Manual/README.md (Original work published 2017)

US EPA, O. (2013, August 1). *Air Quality System (AQS)* [Data and Tools]. US EPA. https://www.epa.gov/aqs

Xie, Y., Paulot, F., Carter, W. P. L., Nolte, C. G., Luecken, D. J., Hutzell, W. T., Wennberg, P. O., Cohen, R. C., & Pinder, R. W. (2013). Understanding the impact of recent advances in isoprene photooxidation on simulations of regional air quality. *Atmospheric Chemistry and Physics*, *13*(16), 8439–8455. https://doi.org/10.5194/acp-13-8439-2013

Xu, J., Shi, J., Zhang, Q., Ge, X., Canonaco, F., Prévôt, A. S. H., Vonwiller, M., Szidat, S., Ge, J., Ma, J., An, Y., Kang, S., & Qin, D. (2016). Wintertime organic and inorganic aerosols in Lanzhou, China: Sources, processes, and comparison with the results during summer. *Atmospheric Chemistry and Physics*, *16*(23), 14937–14957. https://doi.org/10.5194/acp-16-14937-2016

Xu, L., Pye, H. O. T., He, J., Chen, Y., Murphy, B. N., & Ng, N. L. (2018). Experimental and model estimates of the contributions from biogenic monoterpenes and sesquiterpenes to secondary organic aerosol in the southeastern United States. *Atmospheric Chemistry and Physics*, *18*(17), 12613–12637. https://doi.org/10.5194/acp-18-12613-2018

Yang, J., Wen, Y., Wang, Y., Zhang, S., Pinto, J. P., Pennington, E. A., Wang, Z., Wu, Y., Sander, S. P., Jiang, J. H., Hao, J., Yung, Y. L., & Seinfeld, J. H. (2021). From COVID-19 to future

https://doi.org/10.5194/egusphere-2023-749
Preprint. Discussion started: 3 May 2023


electrification: Assessing traffic impacts on air quality by a machine-learning model. *Proceedings of the National Academy of Sciences*, *118*(26). https://doi.org/10.1073/pnas.2102705118

Yarwood, G., Jung, J., Whitten, G. Z., Heo, G., Mellberg, J., & Estes, M. (2010). *Updates to the Carbon Bond Mechanism for Version 6 (CB6)*. 9th Annual CMAS Conference, Chapel Hill, NC.

Zhang, Q., Jimenez, J. L., Canagaratna, M. R., Allan, J. D., Coe, H., Ulbrich, I., Alfarra, M. R., Takami, A., Middlebrook, A. M., Sun, Y. L., Dzepina, K., Dunlea, E., Docherty, K., DeCarlo, P. F., Salcedo, D., Onasch, T., Jayne, J. T., Miyoshi, T., Shimono, A., … Worsnop, D. R. (2007). Ubiquity and dominance of oxygenated species in organic aerosols in anthropogenically-influenced Northern Hemisphere midlatitudes. *Geophysical Research Letters*, *34*(13). https://doi.org/10.1029/2007GL029979

Zhang, X., Cappa, C. D., Jathar, S. H., McVay, R. C., Ensberg, J. J., Kleeman, M. J., & Seinfeld, J. H. (2014). Influence of vapor wall loss in laboratory chambers on yields of secondary organic aerosol. *Proceedings of the National Academy of Sciences*, *111*(16), 5802–5807. https://doi.org/10.1073/pnas.1404727111

Zhao, Y., Nguyen, N. T., Presto, A. A., Hennigan, C. J., May, A. A., & Robinson, A. L. (2016). Intermediate Volatility Organic Compound Emissions from On-Road Gasoline Vehicles and Small Off-Road Gasoline Engines. *Environmental Science & Technology*, *50*(8), 4554–4563. https://doi.org/10.1021/acs.est.5b06247